Journal of Structural Geology, Vol. 11, No. 4, pp. 439 to 455, 1989
Printed in Great Britain

0191-8141/89 $03.00 + 0.00

Thrust fault mechanics and dynamics during a developmental stage of a foreland belt

E. G. BOMBOLAKIS

Department of Geology and Geophysics, Boston College, Chestnut Hill, MA 02167, U.S.A.

(*Received* 5 *April* 1988; *accepted in revised form* 19 *October* 1988)

Abstract—Studies of continental seismogenic zones indicate that deformation during an orogenic stage is episodic and spasmodic down to mid-crustal depths, and that seismic as well as aseismic modes of deformation need to be incorporated in quantitative theories of foreland belts. Such a theory is developed here. It includes a method to help decipher the development of structures such as imbricate fans, frontal ramps and ramp anticlines, as illustrated for the Hogsback frontal ramp and its ramp anticline in the Kemmerer region of the Wyoming Salient.

The structure of the Hogsback ramp is consistent with a shear-fracture origin. Limit equilibrium mechanics indicate that shear failure would have proceeded incrementally, possibly in response to recurring fault slip on the basal décollement. Contrasts in elastic constants and rock strength are critical, e.g. current data indicate that shear-failure development of the ramp would have begun (1) fourth-fifth's distance down the ramp in competent Madison carbonates if they compared in strength with the Marianna limestone, or (2) higher in the section if the Madison compared in strength with the Hasmark or Blair dolostones.

Whether the initial development of the ramp anticline involved seismic modes is not clear yet, but elastic stiffness data indicate that subsequent imbrication of the anticline did involve seismic as well as aseismic modes of deformation.

INTRODUCTION

For many years, the mechanics of fold-and-thrust belts have been analyzed almost exclusively in terms of quasi-static deformation. Recent developments in seismotectonics, however, indicate that seismic as well as aseismic modes of deformation need to be incorporated in mechanical analyses of foreland belts. A prototype fault model consistent with these modes is described and quantified. Then the fault model is related to the structure of a highly documented thrust terrain originally mapped by William Rubey and his colleagues: the classic Kemmerer region of the Wyoming Salient.

The objectives are (1) to extend a preliminary version of the thrust-belt theory (Bombolakis 1986) to a more advanced state, (2) to present a partial test of the theory and (3) to illustrate how several thrust-belt parameters can be calculated from field data not previously utilized. The parameters include relative elastic stiffnesses of the strata calculated from seismic reflection data. These calculations therefore should facilitate predictions of where folding and fracture ought to occur during the development of foreland belts.

SEISMOTECTONIC IMPLICATIONS

Studies of continental seismogenic zones now indicate that deformation during an orogenic stage is episodic and spasmodic down through midcrustal depths (e.g. Allen 1981, Jackson 1983, Savage 1983, Sibson 1983). Seismogenic depths along the compressional zones range from 10 to 15 km or more along the California Coast Ranges, to 20 km under the Transverse Ranges, to 25 km or more along the Zagros, to 50 km or more along the Himalayas. The seismic events are not restricted to Precambrian basement or lower levels. Seismic events can also occur within the sedimentary packages of thrust belts (e.g. Berberian 1982, Davis *et al.* 1983, Namson & Davis 1988). Consequently, seismic as well as aseismic modes of deformation need to be considered in the development of foreland belts where strata are lithified and exhibit pronounced differences in competency, in contrast with those accretionary wedges where the sedimentary packages are poorly indurated when they enter the deformation mill.

Secondly, earthquakes have repeated one another with remarkable reproducibility along specific fault segments (Sieh 1981, Aki 1984, Schwartz & Coppersmith 1984, 1986, Schwartz 1987). A good example in the Tell Atlas thrust terrain is described by Swan (1987). In general, repeatable earthquakes are called *characteristic earthquakes* when the main shocks recur within a narrow range of magnitudes. The fault segments, the barriers to rupture along the fault zone and the distribution of slip on a fault segment—all seem to persist through repeated earthquakes until the geometry and structure of the system are altered sufficiently to accommodate a change in the style of deformation.

Thirdly, some major folds have been growing spasmodically in response to seismic slip on blind thrusts in the California Coast Ranges (Stein & King 1984, Stein 1986, 1987, Wentworth & Zoback 1986, Namson & Davis 1988), on blind reverse faults in the coastal Hawke's Bay region of New Zealand (Hull 1986), and along the El Asnam thrust system in Algeria (King & Veta-Finzi 1981). In the case of the Zagros fold-and-

thrust belt, compression axes of most focal mechanism solutions are perpendicular to major fold axes in Iran (Jackson 1983).

Theories of folding and thrusting, however, have been formulated almost exclusively in terms of slow, continuous, or off-and-on quasi-static deformation, e.g. the critical wedge theories of Chapple (1978), Davis *et al.* (1983), Stockmal (1983), Dahlen *et al.* (1984) and Suppe (1985). Moreover, Woodward (1987) has shown that critical wedge theories do not apply to the Tennessee sector of the Southern Appalachians where adequate field data are available, nor to that part of the Wyoming sector of the Cordilleran belt where the structure is well documented.

Thus, the problems inherent in critical wedge theories are not yet resolved for foreland belts. Furthermore, if the temperature in the hinterland of a foreland belt is close to the melting point, as is the case for a deformed snow wedge in front of a moving snow plow, then deformation in the hinterland could be similar to either the snow plow analog of critical wedge theory, or to the gravitational spreading analysis of Elliott (1976a, 1980). There currently is no hard evidence to determine which of several hypotheses are appropriate for the deep hinterland of a foreland belt. In view of the uncertainties, the following fault model is formulated with respect to specific observations in four areas: earthquake seismology, seismotectonics, well documented portions of thrust belts and laboratory studies.

DESCRIPTION OF FAULT MODEL

Figure 1 depicts a stage of thrust-belt development that is reproduced during piggy-back thrusting. It is characterized by a basal décollement, a frontal ramp and a simple ramp anticline. The fault in Fig. 1 accordingly consists of a lower flat (the basal décollement), the ramp and an upper flat.

In the context of earthquake seismology (Aki 1984), the frontal ramp is regarded as a geometric barrier to rupture propagation of the lower flat beneath the ramp until the geometry and structure of the ramp region are altered sufficiently. Consequently, the thrust sheet initially would be displaced over the ramp to form the simple anticline shown in Fig. 1. Recurring seismic and aseismic slip along the lower flat subsequently would induce further deformation in the ramp region before substantial subhorizontal growth of the lower flat could proceed in the foreland direction beneath the ramp. Several modes of deformation are possible in the ramp region and so, for purposes of illustration, we consider principally the transformation of the simple ramp anticline into an imbricated ramp anticline.

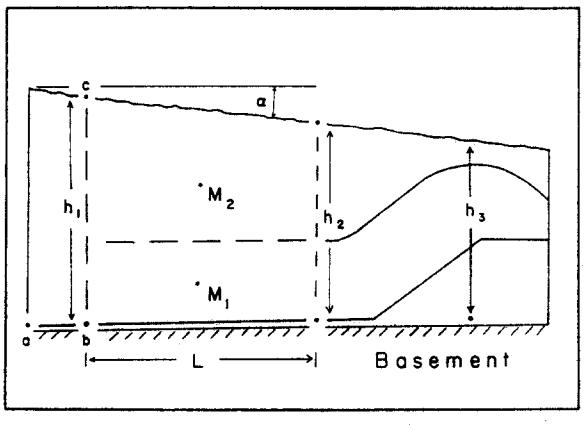

Fig. 1. A developmental stage of a foreland belt. The thrust-belt segment above rupture length L undergoes seismic slip in the foreland direction. The horizontal dashed line subdivides the segment into two main lithotectonic blocks of masses M_1 and M_2. The lower block has a thickness equal to ramp height.

The fault model for this sequence of deformation is as follows. Preseismic creep displacement of hangingwall strata develops along *a–b* of the basal décollement. It produces a tectonic load along *b–c*, leading to a transient stress drop and seismic slip along rupture length L. L is the length of a seismically active thrust-belt segment between two barriers, one of which happens to be a frontal ramp. Several types of barriers are possible, and so the second barrier in the vicinity of *a–b* is not shown. Because L cannot grow substantially in the foreland direction beneath the ramp barrier, preseismic fault creep again develops along *a–b*, and another transient stress drop and repetitive seismic slip recur along nearly the same rupture length. This regimen induces slip of hangingwall strata up the ramp, producing episodic folding and fracture in the ramp region.

The Coalinga anticline is a case in point. The M_L 6.7 Coalinga earthquake occurred on 2 May 1983. An increase of fold amplitude of approximately 0.5 m or more was induced by seismic slip on a blind thrust at approximately 10 km depth (Stein 1987). Seismic profiles indicate that this increase occurred above either a frontal ramp (Namson & Davis 1988) or a set of splay thrusts (Wentworth & Zoback 1986). The postseismic increase of fold amplitude amounted to only 50–60 mm at a decaying rate during the subsequent 2 year period (Stein 1986). Thus, a substantial part of the renewed folding occurred coseismically in response to seismic slip on a complex flat–ramp–thrust system.

The origins of ramps and flats have not been established yet (Bombolakis 1986, Eisenstadt & De Paor 1987). A statistical analysis of major flats in the external portion of the Southern Canadian foreland belt indicates that most of the flats lie within incompetent units, whereas most major ramps cut across stratigraphic sequences that contain dominant competent members (Dahlstrom 1970, Verrall *et al.* 1981). The same relations seem to hold in the Idaho–Wyoming–Utah belt (Royse *et al.* 1975, Dixon 1982, Lamerson 1982), in the Helvetic Nappes (Ramsay 1981), and in substantial portions of the Central and Southern Appalachians (Roeder *et al.* 1978, Woodward 1985, Mitra 1986). Seismic reflection profiles across the North American belts indicate that the basal décollements are not strictly bedding-parallel. They seem to cut up-section regionally at a slight angle to bedding in the foreland direction (Woodward *et al.* 1985). Locally, however, major flats apparently can cut

down-section, perhaps due to competing R_1 and R_2 Riedel shearing in the décollement zone (Platt & Leggett 1986, Woodward *et al.* 1988). In the context of earthquake seismology, the resultant geometrical irregularity would constitute either a barrier or an asperity.

The décollements and detachments within competent sequences are more enigmatic. In a comparison of well exposed mesoscopic ramp–flat systems in several North American belts, Serra (1977, personal communication 1987) observed that flats in carbonate rock typically follow shaly or silty partings. It is not known, however, why the much larger scale flats and detachments in carbonate rock did not originate and remain within nearby incompetent units of a given stratigraphic sequence. Principal examples are the Keystone and Red Spring thrust complexes with décollements within the Bonanza King dolostones instead of the Bright Angel shale (Burchfiel *et al.* 1982), the Heart Mountain detachment fault within the Bighorn Dolomite (Pierce 1987a, b) and the Lochseiten calc-mylonite at the base of the Glarus (Schmid 1975).

In each case, the evidence is negative or inconclusive that abnormal pore pressures were responsible for either the stratigraphic position of the fault or the fault displacements. For example, the 'basal tongues' described by Gretener (1977) may be only minor late-stage phenomena, due to local transient pore pressure increases produced by faulting, or the remnant effects of abnormal pore pressure that triggered faulting. Thus far, the critical role of abnormal pore pressure has been documented in only a very few cases, notably for the high-angle Rangely fault (Raleigh *et al.* 1976) and for the low-angle Hartford dike detachment slide (Bombolakis 1981). Thus, the characterization of fault behavior must be restricted to empirical observations of active faults until adequate information accumulates on the various physico-chemical processes of faulting illustrated by Chester (1985),Gilotti & Kumpulainen (1986), Wojtal & Mitra (1986), Logan (1987) and Schmid *et al.* (1987).

In conformity with Bombolakis (1986), the fault model is defined for the segment bounded in Fig. 1 by the vertical dashed lines h_1 and h_2, topographic slope angle α and rupture length L, where the horizontal dashed line subdivides the segment into two major lithotectonic units: a lower block of mass M_1 with thickness equal to ramp height and an upper block of overlying strata of mass M_2. The lower block typically includes more competent strata than the upper block. As will be seen, the following quantification of this fault model is independent of whether abnormal pore pressure is the parameter that triggers fault slip.

QUANTIFICATION OF THE FAULT MODEL

The fault model in Fig. 1 is quantified in Fig. 2. The lower block in Fig. 2(a) is defined by mass M_1 over rupture length L. The block of overlying strata is defined by mass M_2 for length L and topographic slope angle α. A common observation in foreland belts is that the net

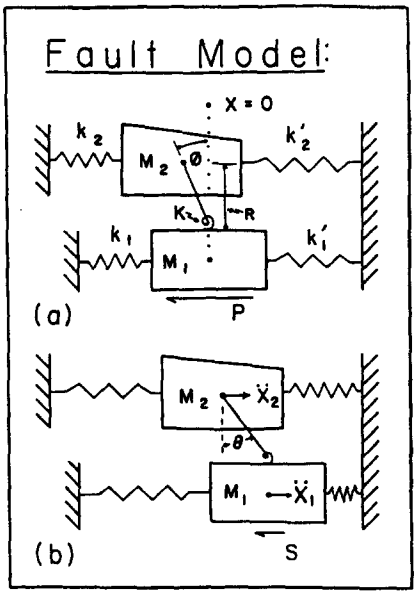

Fig. 2. Fault model of the thrust-belt segment above rupture length L in Fig. 1. The fault model, at the verge of stick–slip in (a), undergoes seismic slip in (b) with a stress drop from P to S.

slip of a thrust sheet varies in the strike direction, e.g. by the 'bow-and-arrow' rule of Elliott (1976b). Consequently, the thrust-belt segment in Fig. 2 is defined to be of unit width W perpendicular to the diagram, for future analyses of slip variation in the strike direction.

In a manner similar to the elastic rebound theory, preseismic creep compresses the k_1 and k_2 springs, and deflects torsion spring K through angle ϕ, potentially compressing the k_1' and k_2' springs, with the result that the basal shear stress at the bottom of block M_1 approaches its limiting value P. The elastic constants k_1, k_1', k_2, k_2', and torsion constant K are calculated with seismic and stratigraphic data, thereby taking facies changes and contrasts of rock properties into account.

The configuration illustrated in Fig. 2(a) corresponds to the tectonic situation in which the subhorizontal elastic tectonic strain increases with depth down to the basal décollement. If we define X_1 and X_2 as the horizontal co-ordinates of M_1 and M_2, respectively, then the relative elastic displacement between the blocks at the verge of stick–slip is $X_1 - X_2 = R\phi$. However, the additional physical possibilities for ϕ are that $\phi = 0$ or that ϕ is a clockwise angle instead of a counterclockwise angle with respect to the dotted reference line $X = 0$. For generality therefore, ϕ is defined positive when measured counterclockwise as shown, and negative when measured clockwise. For each case, $X_2 = -R\phi$ if we choose the co-ordinate system with $X_1 = 0$ when the system is at the verge of stick–slip. These definitions involve no additional physical assumptions, except with respect to the radius of gyration R.

The radius of gyration is a fundamental concept in Newtonian mechanics (e.g. Frank 1939, p. 168) that enables a body of complicated geometry to be replaced by a simpler body to facilitate mechanical analyses. The upper block of mass M_2 in Fig. 1 has a complex geometry, but it can be replaced by a mass point at a distance R by

calculating its moment of inertia with respect to the top of the lower block. Because R is larger than the vertical distance measured from the horizontal dashed line to the center of mass M_2 in Fig. 1, the blocks are shown schematically in Fig. 2 as if they were separated. But since they actually are in mutual contact, the average internal shear along the horizontal dashed line in Fig. 1 is characterized by the distortion of the torsion spring of elastic constant K at the other end of R in Fig. 2. Thus, the radius of gyration also serves as the moment arm of the torque exerted by the upper block on the lower block.

The basal shear stresses are not constant along the fault surface in Fig. 2, nor along a comparable segment of an actual fault. Therefore, their effects are calculated in terms of their average values. When the average basal shear stress reaches its limiting value P in Fig. 2(a), a rapid transient stress drop occurs from P to S, with stick–slip motion in Fig. 2(b). There, $\ddot{X}_1$ is the acceleration of the lower block, and $\ddot{X}_2$ is the acceleration of the upper block. $\theta = \phi$ when stick–slip begins. The horizontal displacements X_1 of M_1 and X_2 of M_2 are positive when measured to the right of the dotted reference line $X = 0$ in Fig. 2(a).

Both P and S can be related directly to the time-predictable and slip-predictable models of recurring earthquakes (Shimazaki & Nakata 1980, Mogi 1985). In the time-predictable model, P has a constant recurring value of the peak strength, whereas S varies in value from one earthquake to the next. In the slip-predictable model, S has a constant recurring value of the residual strength, whereas it is P that varies in value from one earthquake to the next. Because of the uncertainties regarding P and S, we focus attention on their difference $(P - S)$. The difference is directly proportional to the average stress drop calculated in earthquake seismology (Bombolakis 1986).

The equations of motion are obtained from the free-body diagrams of the model in Fig. 3. Horizontal forces are positive when they act towards the right in the positive X-direction; negative in the opposite direction. Since the system in Fig. 2(a) is at the verge of stick–slip, the basal shear force in Fig. 3(a) equals $-PLW$. The force exerted by each linear spring during this stage is its spring constant times the value of displacement ξ imposed by preseismic creep. A force of magnitude $K\phi/R$ also is associated with precursory torsion, where $K\phi$ is the torque and R is the moment arm. Since the sum of the forces on each block must equal zero in Fig. 3(a), we have two equations that enable the preseismic creep to be expressed quantitatively in terms of the precursory internal shear $K\phi/R$ and the basal shear PLW.

As soon as seismic slip begins, the forces in Fig. 3(a) transform to those in Fig. 3(b). The sum of the forces on each block now equals mass × acceleration. Therefore, by means of the four equations shown in Fig. 3, the equations of motion can be expressed as

$$M_1\ddot{X}_1 + (k_1 + k_1' + K/R^2)X_1 - (K/R^2)X_2 = (P - S)LW + K\phi/R \quad (1)$$

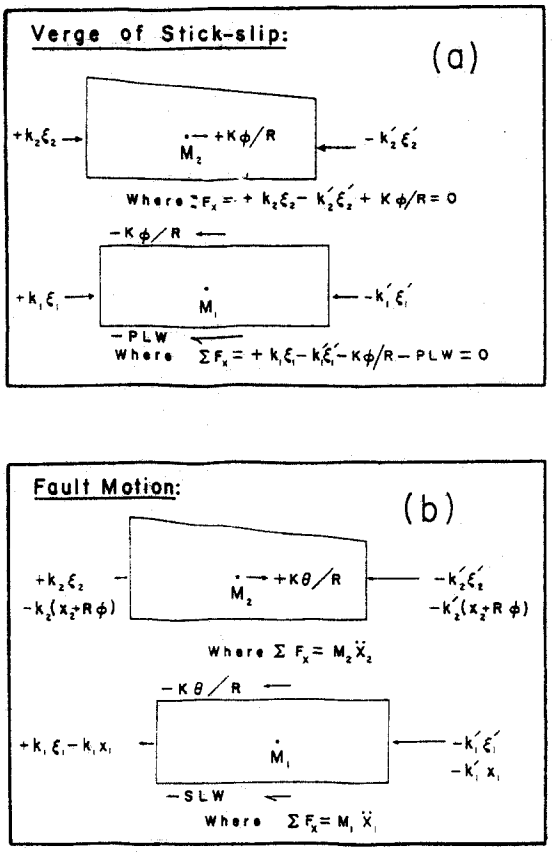

Fig. 3. Free-body diagrams of the horizontal forces acting on the fault model.

and

$$M_2\ddot{X}_2 + (k_2 + k_2' + K/R^2)X_2 - (K/R^2)X_1 = -(k_2 + k_2' + K/R^2)R\phi \quad (2)$$

using the geometric relation that $R\theta = X_1 - X_2$. These equations reduce, respectively, to equations (1) and (2) of Bombolakis (1986) for the special case of $\phi = 0$. (The sign of the third term of equation 2 in the 1986 paper should be minus instead of plus, a typographic error.)

The equations of motion are coupled non-homogeneous differential equations. Their general solution consists of two parts: the homogeneous solution plus the particular solution. The homogeneous solution is derived for the case in which the sum of the terms on the left-hand side of each equation is set equal to zero. This homogeneous solution actually corresponds to the general solution of the mechanical analog in coupled oscillator theory (Symon 1971) shown in Fig. 4.

Two masses M_1 and M_2 are connected in series by three linear springs in Fig. 4, where they undergo horizontal oscillatory motion. Symon (1971, p. 192) shows that their equations of motion are

$$M_1\ddot{X}_1 + (k_1^* + k_2^*)X_1 + k_3^*X_2 = 0 \quad (3)$$

and

$$M_1\ddot{X}_2 + (k_2^* + k_3^*)X_2 + k_3^*X_1 = 0. \quad (4)$$

The mathematical analogy between Fig. 4 and the homogeneous case for Fig. 2 is effected by re-writing equations (1) and (2) as

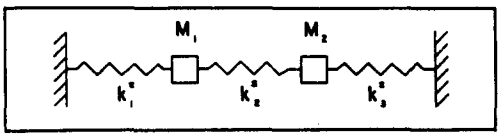

Fig. 4. Analog model used for the homogeneous solution of the fault model problem in Fig. 2.

$$M_1\ddot{X}_1 + k_1''X_1 + k_3''X_2 = 0 \tag{5}$$

and

$$M_2\ddot{X}_2 + k_2''X_2 + k_3''X_1 = 0, \tag{6}$$

where

$$\left.\begin{aligned} k_1'' &= k_1 + k_1' + K/R^2 \\ k_2'' &= k_2 + k_2' + K/R^2 \\ k_3'' &= -K/R^2 \end{aligned}\right\}. \tag{7}$$

Therefore, the homogeneous solution (Symon 1971, equations 4.160 and 4.161) for equations (1) and (2) is

$$X_1^h = A_1 \cos(\omega_1' t + \theta_1) - \frac{\Delta\omega^2}{2K^2}\sqrt{\frac{M_1}{M_2}} \times A_2 \cos(\omega_2' t + \theta_2) \tag{8}$$

and

$$X_2^h = \frac{\Delta\omega^2}{2K^2}\sqrt{\frac{M_1}{M_2}} A_1 \cos(\omega_1' t + \theta_1) + A_2 \cos(\omega_2' t + \theta_2), \tag{9}$$

where A_1, A_2, θ_1 and θ_2 are the constants of integration. They are evaluated with the initial conditions in Fig. 2 after the general solution of (1) and (2) is obtained. Consequently, we proceed to the particular solution as follows. First, equations (1) and (2) are divided through, respectively, by M_1 and M_2. Note that these equations now are expressed in the traditional form of non-homogeneous equations with constant coefficients where the coefficient of the first derivative term in each equation is zero, and where the terms on the right-hand sides of the equations are constants. Secondly, $\ddot{X}_1$ and $\ddot{X}_2$ are each set equal to zero for a particular case (e.g. Murphy 1960, p. 146). Third, the two equations in this form are solved simultaneously for the particular solution X_1^p of equation (1) and X_2^p of equation (2). The result is

$$X^p{}_1 = \frac{k_2 + k_2' + K/R^2}{B}(P - S)LW \tag{10}$$

and

$$X^p{}_2 = \frac{K/R^2}{B}(P - S)LW - R\phi, \tag{11}$$

where

$$B = (k_1 + k_1')(k_2 + k_2') + (k_1 + k_1' + k_2 + k_2')K/R^2. \tag{12}$$

In summary, then, the general solution for a variety of initial conditions in Fig. 2 is

$$X_1 = X_1^h + X_1^p, \quad X_2 = X_2^h + X_2^p, \tag{13}$$

where, following Symon (1971), the natural frequencies are

$$\omega_1' = \sqrt{\omega_{10}^2 + \tfrac{1}{2}\Delta\omega^2}, \quad \omega_2' = \sqrt{\omega_{20}^2 - \tfrac{1}{2}\Delta\omega^2} \tag{14}$$

with

$$\omega_{10} = \sqrt{\frac{k_1 + k_1' + K/R^2}{M_1}}, \quad \omega_{20} = \sqrt{\frac{k_2 + k_2' + K/R^2}{M_2}} \tag{15}$$

$$\Delta\omega^2 = \pm 2K^2 \quad \text{when } \omega_{10} = \omega_{20} \tag{16}$$

$$\Delta\omega^2 = (\omega_{10}^2 - \omega_{20}^2)\left\{\left[1 + \frac{4K^4}{(\omega_{10}^2 + \omega_{20}^2)^2}\right]^{1/2} - 1\right\} \quad \text{when } \omega_{10} \neq \omega_{20} \tag{17}$$

$$K^2 = \frac{k_3''}{\sqrt{M_1 M_2}} = -\frac{K/R^2}{\sqrt{M_1 M_2}}. \tag{18}$$

We choose the negative sign in (16) because (18) is negative, noting that ω_1' is the higher frequency when $\omega_{10} \geq \omega_{20}$, whereas ω_2' is the higher frequency when $\omega_{10} < \omega_{20}$. Here ω_{10} and ω_{20} are the natural frequencies of horizontal oscillation that the lower and upper blocks, M_1 and M_2, would have, respectively, if each block were a simple harmonic oscillator moving independently of each other. The result is that the motion of each block involves its own distinct combination of the natural frequencies in (14).

The constants of integration (A_1, A_2, θ_1 and θ_2) now can be determined from the initial conditions in Fig. 2. There is no loss of generality in assuming that stick–slip begins at reference time $t = 0$. The initial conditions are that the displacements are $X_1 = 0$ and $X_2 = -R\phi$ at $t = 0$, and that the initial velocities are $\dot{X}_1 = 0$ and $\dot{X}_2 = 0$. The displacement equations are given in (13), and the velocity equations are obtained by differentiating equations (13) once with respect to time. Substituting the initial conditions into these four equations, we find that

$$\theta_1 = 0, \quad \theta_2 = 0 \tag{19}$$

$$A_1 = \frac{[\Delta\omega^2 - 2\omega_{20}^2]M_2}{2B\left[\left(\frac{\Delta\omega^2}{2K^2}\right)^2 + 1\right]}(P - S)LW \tag{20}$$

and

$$A_2 = \frac{\left[\Delta\omega^2\left(\frac{\omega_{20}}{K}\right)^2 + 2K^2\right]\sqrt{M_1 M_2}}{2B\left[\left(\frac{\Delta\omega^2}{2K^2}\right)^2 + 1\right]}(P - S)LW. \tag{21}$$

To determine the net slip of a stick–slip event, we need to consider the duration time of the lower block's motion. The velocity of the lower block decreases to zero at the end of a stick–slip event, whereas the upper block continues to oscillate until damping terminates the

ground motion. Therefore, by differentiating X_1 of equations (13) once with respect to time, then setting the resulting velocity equation equal to zero, the *duration time equation* is found to be

$$\cos \omega_2' t_d = \pm \sqrt{1 - \frac{2K^2 \omega_1' A_1 M_1}{\Delta\omega^2 \omega_2' A_2 M_2} \sin^2 \omega_1' t_d}, \quad (22)$$

where t_d is the duration time of stick–slip. This equation is solved implicitly for t_d when the other parameters are calculated from field data. Substitution of its value into the equation for X_1 automatically determines the *dynamic net slip equation* as

$$\overline{X}_1 = A_1 \cos \omega_1' t_d - \frac{\Delta\omega^2}{2K^2} \sqrt{\frac{M_1}{M_2}} A_2 \cos \omega_2' t_d + \frac{k_2 + k_2' + K/R^2}{B} (P - S)LW, \quad (23)$$

where $\overline{X}_1$ is the net slip.

When this net slip is achieved, the motion of the upper block transforms from a state with natural frequencies ω_1' and ω_2' to a state with a natural frequency of

$$\omega_{20} \simeq \sqrt{(k_2 + k_2' + K/R^2)/M_2}. \quad (24)$$

This transformation occurs because the upper block of the prototype model becomes a simple harmonic oscillator when the lower block becomes immobilized (cf. equation 7 of Bombolakis 1986). The equal sign applies in equation (24) when the damping is constant, as in the case of Coulomb frictional damping. The approximate sign applies when the damping is moderately velocity dependent, as in the case of weak viscous damping.

During an earthquake, the ground motions involve a much broader spectrum of frequencies than does the geologic fault model in its present state of development. Theoretically, every continuous body is associated with an infinite number of frequencies. In practice, the high frequencies are damped out more rapidly than the low frequencies, and seismographs usually are designed for response in the lower range, e.g. the 10 Hertz range. Because the model here is a prototype, a comparison is made between the geologic fault model and traditional crack models in seismology.

COMPARISON WITH SEVERAL CRACK MODELS IN SEISMOLOGY

The geologic fault model in Fig. 2 differs in several important ways from the traditional crack models employed in earthquake seismology. The geologic model includes analyses of fault-slip velocity and stratigraphic anisotropy, but not rupture velocity, whereas the traditional crack models are formulated in terms of the rupture velocity of a spreading crack in isotropic media. Despite these differences, there is almost a one-to-one correspondence between the equations of net slip amongst these models for the condition of isotropy and for a simple case of stratigraphic anisotropy.

The simplest case of stratigraphic anisotropy occurs when both blocks in Fig. 2 have the same physical properties that change laterally due to a facies change in the foreland direction. For this case, $M_1 = M_2 = M$, $k_1 = k_2 = k$ and $k_1' = k_2' = k'$, but $k \neq k'$. For this case, equation (23) reduces to

$$\overline{X}_1 = \frac{(P - S)LW}{2(k + k')} \left[(1 - \cos \omega_2' t_d) + \left(\frac{\omega_2'}{\omega_1'}\right)^2 (1 - \cos \omega_1' t_d) \right], \quad (25)$$

where

$$\omega_1' = \sqrt{\frac{k + k' + 2K/R^2}{M}}, \quad \omega_2' = \sqrt{\frac{k + k'}{M}}.$$

This equation, in turn, reduces to equation (3) of Bombolakis (1986) for the isotropic case of $k = k'$. In both cases, damping of block motion along the fault is constant, analogous to Coulomb damping (see Den Hartog 1956, pp. 362–363) because the residual strength S is assumed constant during seismic fault slip.

According to equation (25), the seismic net slip is directly proportional to the ratio of stress drop $(P - S)$ and rupture length L with respect to the elastic constants, keeping in mind that W is only a unit width and that cosine functions are limited in value from +1 to −1. For comparison, the net slip equation for traditional crack models in earthquake seismology is

$$U = \frac{\Delta\sigma \sqrt{A}}{C\mu}, \quad (26)$$

where U is the average coseismic net slip (Kanamori & Anderson 1975).

This equation shows that U is proportional to the ratio of the average stress drop $\Delta\sigma$ and the square root of rupture area A with respect to the rigidity modulus μ. C is a dimensionless factor that depends on the shape of the spreading crack. The square root of A, of course, is proportional to rupture length L. Consequently, there is a good cross-correlation in this instance between the geologic fault model and traditional crack models in seismology.

EVALUATION OF FAULT PARAMETERS

One of the most important relations in seismology is the seismic moment of the earthquake. According to elastic dislocation theory (Kanamori & Anderson 1975), the amplitude of very long-period waves is proportional to

$$\mathbf{M}_0 = \mu U A. \quad (27)$$

Seismic moment $\mathbf{M}_0$ also is related to E_s, the seismic energy of radiation, by

$$E_s \approx (\Delta\sigma/2\mu)\mathbf{M}_0, \quad (28)$$

where μ usually is taken to be (3–5) $\times 10^{11}$ dynes cm^{-2} and equation (26) provides an estimate of $\Delta\sigma$ (Kanamori 1977). Brune (1968) shows how average seismic slip

rates can be calculated from the summation of seismic moments. His method therefore provides a potential means of partitioning geologic strain rates into seismic and aseismic modes because energy estimates have been made for some of the aseismic modes by Elliott (1976b) and by Mitra & Boyer (1986), and for some of the seismic modes by Kanamori (1977) and Sibson (1980).

One of the principal difficulties here is that the details of the rupture process cannot be seen clearly through the long-period window where the seismic moment is observed (Aki 1983). The few strong-motion studies that have been made in the near field indicate that the rupture process is more complex than previously thought. Therefore, an analysis of the fault parameters in net slip equation (23) should provide information on some of the details. This equation indicates that the relevant fault parameters for a given rupture length include masses M_1 and M_2, their various spring constants and the radius of gyration.

The equations for these parameters are derived in a forthcoming paper (Bombolakis in preparation). The radius of gyration is found to be

$$R = \sqrt{\frac{L^2 \sec^2 \alpha}{12} + \frac{H^2}{3}} \tag{29}$$

by calculating the moment of inertia $I = M_2 R^2$ of the upper block with respect to the top of the lower block of mass M_1 in Fig. 2. Equation (29) reduces to the equation for a rectangular block given by Den Hartog (1948, p. 225), i.e. when $\alpha = 0$. Consequently, R accounts for rupture length L of the basal décollement, topographic slope angle α of the thrust belt and the average vertical thickness H of the upper block in Fig. 2. It is one of the parameters that determine both the coseismic net slip and the fundamental frequencies of the system.

R also is one of the parameters that determine torsion constant K. The torsion constant per unit width W is

$$K/W \approx \frac{E_{\text{avg.}} L}{2(1 + \nu_{\text{avg.}})} R, \tag{30}$$

where $E_{\text{avg.}}$ and $\nu_{\text{avg.}}$, respectively, are the average values of Young's modulus E and Poisson's ratio ν for the upper block in Fig. 2. The simplest way to estimate the elastic constants is to utilize data from seismic profiling. The data include density ρ, P-wave velocity, V_p, and S-wave velocity, V_s, where

$$E = \rho\left[\frac{3V_p^2 - 4V_s^2}{(V_p/V_s)^2 - 1}\right] \tag{31}$$

$$\nu = \frac{1}{2}\left[1 - \frac{1}{(V_p/V_s)^2 - 1}\right]. \tag{32}$$

The other spring constants in Fig. 2 are the composite spring constants of four stratigraphic sequences located along the fore-and-aft ends of the fault model. These sedimentary packages are defined by their thicknesses, unit width W, and a common bed length $l_0 \ll L$. Each of the four packages supports its own distinct set of stresses during a precursory stage. Thus, the stress in a given bed has to vary along length L of the fault model. But since $l_0 \ll L$, the stress in each bed is locally uniform over length l_0, or nearly so. For these conditions, the effective bed stress $\bar{\sigma}_{xx}$ acting in the tectonic direction along each length l_0 is given approximately by

$$\bar{\sigma}_{xx} \approx \frac{\nu}{1 - \nu} \rho g y_0 (1 - \lambda) + \delta \rho g y_0 (1 - \lambda) + \frac{E \alpha_T}{1 - \nu} \Delta T + \frac{E}{1 - \nu^2} \varepsilon_{xx}, \tag{33}$$

where y_0 is the depth of the bed at one of the fore-and-aft end points.

Each term on the right-hand side of (33) represents a specific physical contribution to the bed stress. The first term is the lateral effective stress component due to overburden pressure $\rho g y_0$ and the Hubbert–Rubey fluid pressure ratio λ. It is derived in the same manner as equation (3) of Jaeger & Cook (1969, p. 356). The second term takes into account the elastic anisotropy that was induced by compaction during the burial history of the bed, where the anisotropic parameter δ is calculated from seismic profiling data in the manner shown by Thomsen (1986). The effects of topography on these two terms appear to be minimal, except at rather shallow depths (Bauer *et al.* 1985). The third term is the stress due to the geothermal gradient, where α_T is the linear coefficient of thermal expansion and ΔT is the difference in temperature between the ground surface and depth y_0 under steady-state conditions. Therefore the first three terms, in conjunction with the effective overburden pressure, represent a reference state of non-tectonic stress that is more appropriate than Heim's Rule (see McGarr & Gay 1978, pp. 431–432, and Suppe 1985, p. 184). The fourth term is the tectonic stress in the transport direction. It is produced by a tectonic elastic strain ε_{xx} that may vary with depth along the fore-and-aft vertical boundaries of the fault model. The horizontal effective normal stress $\bar{\sigma}_{zz}$ in the perpendicular direction has an equation essentially the same as (33), differing only in the coefficient of the fourth term; viz., with a coefficient $(\nu E)/(1 - \nu^2)$. The application of these equations is illustrated by $\bar{\sigma}_{EW}$ and $\bar{\sigma}_{NS}$ in figs. 3 and 4 of Bombolakis (1986) for the special case of $\delta \approx 0$ and $\alpha_T \approx 0$.

The linear spring constant of each bed at the fore-and-aft boundaries of the model, per unit width, is

$$k_i/W = \frac{E_i}{1 - \nu_i^2} \frac{h_i}{l_0}, \tag{34}$$

where h_i is the thickness of bed i. From the standpoint of seismic stratigraphy, bed i is the interval velocity thickness over which the elastic constants E_i and ν_i are determined from seismic profiling data. Therefore, for n beds or for n interval velocity thicknesses in a sedimentary package, there are n equations of this form.

These n equations enable a composite spring constant k_{ss} to be calculated for a sedimentary package. A surprising feature of k_{ss}, however, is that it is not solely a function of the various k_i. It also is a function of how the elastic tectonic strain varies with depth. *In situ* stress

measurements indicate that the stresses in intact competent rock increase more or less linearly with depth (Haimson 1977, McGarr & Gay 1978). Fluctuations have been traced in some cases to differences in the elastic constants of contrasting rock types (McGarr & Gay 1978, Haimson personal communication 1987). Consequently, the case considered here is that the elastic tectonic strain increases linearly with depth in each sedimentary package at the fore-and-aft ends of the fault model.

Most methods of *in situ* stress measurement measure strains. Suppose, therefore, that a value ε_0 of the tectonic strain can be estimated for the uppermost bed of a sedimentary package, and that the *in situ* data indicate that this value of ε_{xx} increases at a constant rate m with depth. The composite spring constant per unit width for these conditions is

$$\frac{k_{ss}}{W} = \frac{1}{W} \frac{\sum_{i=1}^{n} k_i(md_i + \varepsilon_0)}{m\left[\sum_{i=1}^{n} k_i(md_i + \varepsilon_0)d_i \Big/ \sum_{i=1}^{n} k_i(md_i + \varepsilon_0)\right] + \varepsilon_0}, \tag{35}$$

where d_i is the relative depth position of bed i within the sedimentary package.

An important special case occurs when the elastic tectonic strain is nearly constant with depth. For this condition, $m = 0$, with the result that

$$\frac{k_{ss}}{W} = \frac{1}{W} \sum_{i=1}^{n} k_i. \tag{36}$$

It is the same equation given by Den Hartog (1956, p. 36) for his composite spring constant. The important feature of this equation is that it can be used to estimate (35) without having to know the values of ε_0 and m. We need only interpret ε_0 as the average value of the elastic tectonic strain in the sedimentary package. Thus, when the elastic tectonic strains are not known, the composite spring constants k_1, k_1', k_2 and k_2' in Fig. 2 can be estimated directly with seismic reflection profiling data, using equations (31), (32), (34) and (36). These concepts are illustrated next with respect to a well documented thrust terrain in Wyoming.

KEMMERER REGION OF THE WYOMING SALIENT

Synorogenic conglomerates in the Idaho–Wyoming–Utah fold-and-thrust belt indicate that thrust faulting proceeded episodically, in a stop-and-go fashion, on both the grand scale and the scale of a single thrust system (Armstrong & Oriel 1965, Royse *et al.* 1975, Lamerson 1982, Wiltschko & Dorr 1983). Figure 5 is a reference map of this belt. The major thrusts are progressively younger from west to east. Here, we consider the classic Kemmerer region with respect to the fault model. The major thrusts in this locale are the Absaroka thrust (A) and the Hogsback thrust (H).

The Absaroka thrust is one of the earliest great thrusts discovered in North America. It is carried piggyback by the Hogsback. Cross-sections of the Absaroka were constructed along BB′ through GG′ of fig. 5 by Rubey *et al.* (1975) prior to modern seismic profiling and extensive drilling. Since then, a cross-section that extends easterly along and beyond section 6, across both the Absaroka and Hogsback thrusts, has become one of the most highly constrained balanced cross-sections in the Wyoming Salient, largely through the efforts of Lamerson (1982, 1985), supplemented by Delphia & Bombolakis (1988). Special attention therefore is focused on this cross-section after we consider the seismic profile of

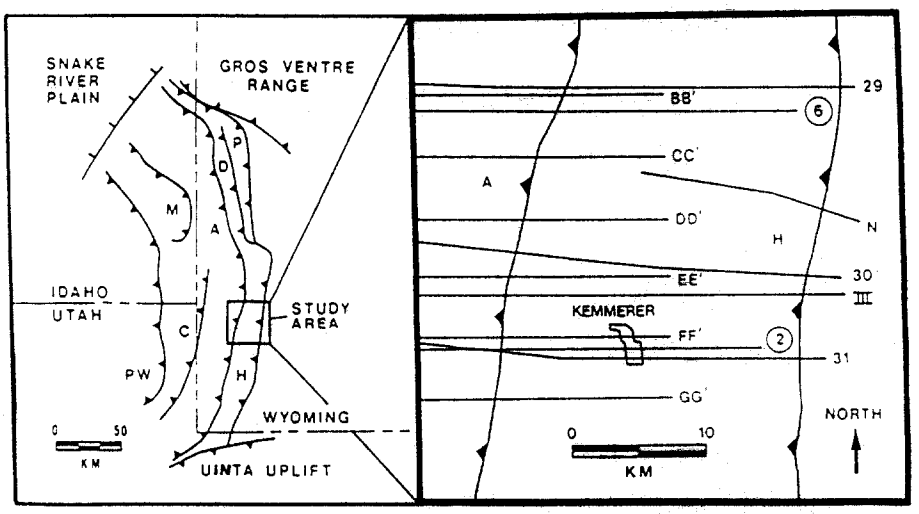

Fig. 5. Reference map of the Idaho–Wyoming–Utah foreland belt. A = Absaroka thrust, C = Crawford thrust, D = Darby thrust, H = Hogsback thrust, M = Meade thrust, P = Prospect thrust and PW = Paris–Willard thrust. The enlargement on the right shows the locations of published cross-sections within the Kemmerer region. Sections BB′, CC′, DD′, EE′, FF′ and GG′ are presented by Rubey *et al.* (1975). Section N is given by Norton (1983), and section III corresponds to Plate III of Royse *et al.* (1975). Sections 2 and 6 correspond, respectively, to Plates 2 and 6 of Lamerson (1982). Sections 29, 30, and 31 are published by Dixon (1982) in generalized form.

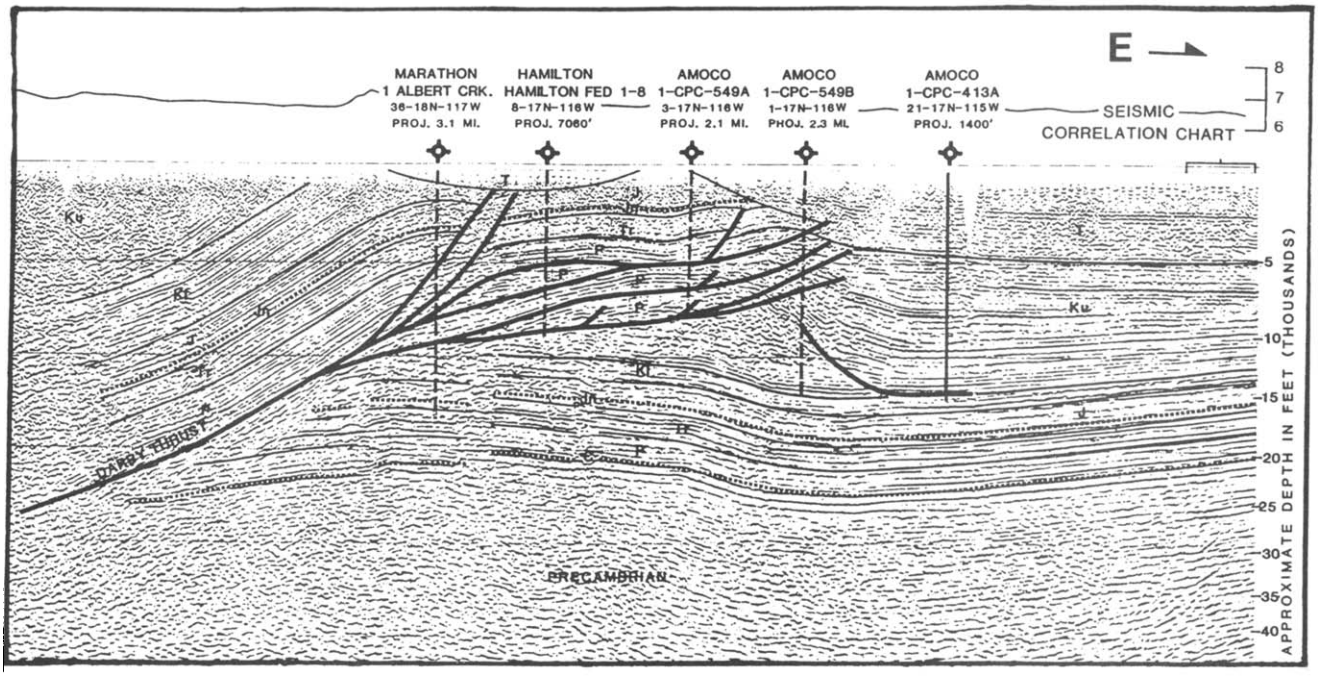

Fig. 6. Seismic section of the Hogsback frontal ramp, located approximately 40 km south of Kemmerer. (Darby thrust ≡ Hogsback thrust.) From fig. 5 of Williams & Dixon (1985).

Williams & Dixon (1985), located 40 km south of Kemmerer. Both sections are subparallel, spaced some 55 km apart, and cut across the Hogsback ramp.

Some vital clues to the origin of the Hogsback ramp are revealed in Figs. 6–8. Figure 6 is part of the seismic reflection profile by Williams & Dixon (1985). No attempt was made to identify every fault in the imbricate zone, and so the representation of the overthrust complex is relatively schematic. However their seismic picture of the ramp footwall strata is observed commonly in seismic profiles across the belt (Dixon personal communication 1987, Lamerson, personal communication 1987 and see seismic profile of Norton 1983). Consequently, this picture frequently was interpreted as an anticlinal structure during hydrocarbon exploration. If correct, we would have to consider that the origin of the frontal ramp probably was related to folding processes, and not simply due to compression-induced brittle shear fracture. Extensive drilling along the belt, however, has demonstrated that the picture of the ramp footwall strata illustrated in Fig. 6 is usually the result of a velocity pullup.

Figure 7 shows the seismic profile of the ramp footwall strata corrected with well data by Williams & Dixon (1985). Their cross-section now indicates that the Hogsback frontal ramp developed in a semi-brittle man-

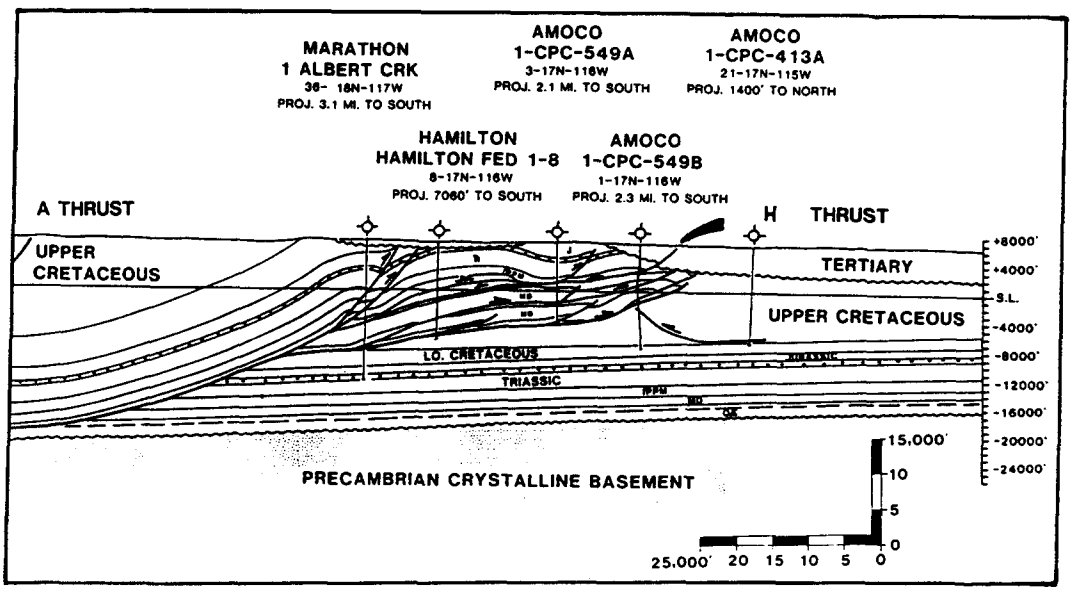

Fig. 7. Cross-section showing the structure of the ramp footwall in Fig. 6 corrected with well data by Williams & Dixon (1985), from their fig. 10.

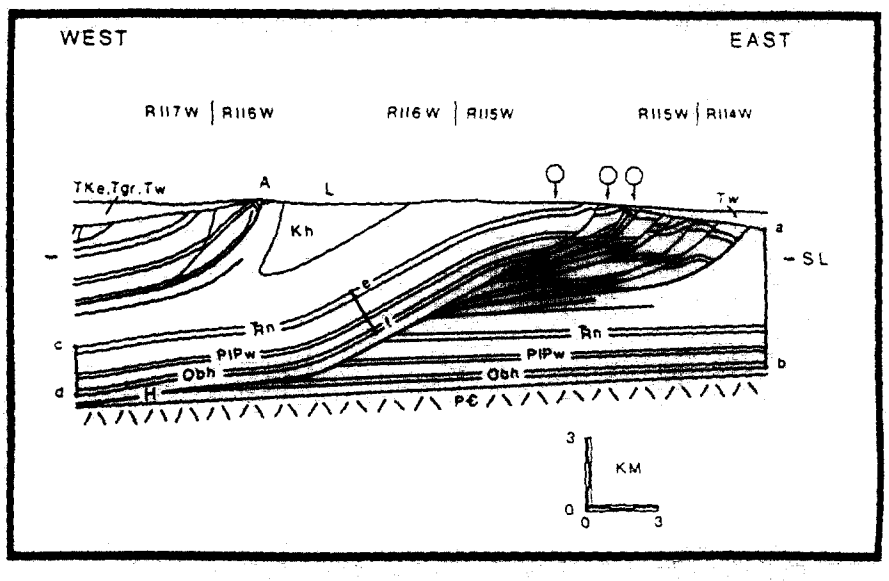

Fig. 8. Balanced cross-section of the Absaroka (A) and Hogsback (H) thrust sheets, 15 km north of Kemmerer. It is co-linear with section 6 in Fig. 5, and extends as far east as section 29 in Fig. 5. The three key marker beds are Ordovician Bighorn dolomite (O_{bh}), Permo-Pennsylvanian Weber sandstone-PIP_w) and Triassic Nugget sandstone (T_{Rn}). The Lazeart syncline (L) is demarcated by a solid-line curve drawn along contact between Frontier Formation and Cretaceous Hilliard clastic sequence (K_h). Reference line e–f transforms to e'–f' in Fig. 10 during palinspastic restoration. From Delphia & Bombolakis (1988).

ner. Diagnostic features are: (1) relatively undeformed competent strata in the ramp footwall; (2) the fact that the ramp is sharply defined in seismic profiles; and (3) the almost 30° angle that the ramp makes with bedding in the footwall.

These observations indicate that the ramp developed by shear fracture due to subhorizontal compression. A single spreading fracture, however, would have been blunted by incompetent beds within the predominantly competent sequence. The weak beds include members of the Ankareh, Woodside and Dinwoody Formations, and soft shales of the Gannett Formation above the predominantly competent sequence (Table 1). The ramp therefore must have developed progressively by sequential incremental fracture of the competent beds, with localized shearing across the interbedded incompetent members.

Figure 8 reveals the same features of the Hogsback ramp and ramp footwall strata illustrated in Fig. 7, and several additional important features. L is the Lazeart syncline—a major fold more than 70 km in length—adjacent to the Hogsback ramp. The three open circles indicate three wells close to the section, wells in which unusually extensive dip meter data provide critical control for defining the geometry of the imbricated ramp anticline. Delphia & Bombolakis (1988) demonstrate that most of the imbricates had formed in the break-back sequence, i.e. sequentially in the hinterland direction. Three key beds of the predominantly competent sequence are delineated to facilitate discussion of the structure. They are the Ordovician Bighorn dolomite, the Permo-Pennsylvanian Weber sandstone and the Triassic Nugget sandstone.

According to the geologic fault model in Fig. 2, recurring basal slip stores elastic strains temporarily in the frontal zone. Recurrence intervals of repeatable earthquakes range from a few tens of years to a few hundred years to several thousand years (Schwartz & Coppersmith 1986). The longer the interseismic interval, the longer the time for aseismic modes to dissipate the elastic strains. Overprinting by aseismic modes such as cleavage development and pressure solution accordingly can make analyses of mechanical evolution highly complicated. For this reason, the Kemmerer region is appropriate for a first attempt at this type of analysis. The strata exhibit no significant metamorphism (Rubey *et al.* 1975, Mitra & Yonkee 1985). A remarkable feature observed independently by Dixon (1982) and Lamerson (1982) is that the predominantly competent sequence, just above the basal décollement, extends westward 30 km beyond *c–d* of Fig. 8 with no deformation apparent within the resolution of current subsurface data.

I therefore consider the possibility that the Hogsback frontal ramp resulted from recurring slip of the thrust-belt segment along rupture length L in Fig. 1, and predict where shear failure should have been initiated within the predominantly competent sequence to form the Hogsback ramp. This problem is analyzed as a function of: (1) effective overburden pressure; (2) the geothermal gradient; (3) contrasts of the elastic constants; (4) competency contrasts; and (5) the elastic tectonic strain gradient with depth. For a first analysis, a standard fluid pressure gradient with depth is adopted with a Hubbert–Rubey fluid pressure ratio of $\lambda = 0.435$. A geothermal gradient of 20°C km^{-1} is based on the data of Warner & Royse (1987). The analysis then is applied to two cases: (1) the case of an elastic tectonic strain that is constant with depth down to the level of the basal décollement, in a manner somewhat similar to the horizontal strain induced initially in compressional sandbox experiments; and (2) for the case of an elastic tectonic strain that increases linearly with depth.

Table 1. Data for limit equilibrium mechanics of initial development of the Hogsback frontal ramp, assuming a shear-failure origin in response to fault slip on the basal décollement, and Hubbert–Rubbey fluid pressure ratio of 0.435 for permeable strata

Stratigraphic unit, depth (km) to middle of unit*	Elastic constants† E, ν, α_T	Mohr envelope strength criteria‡ Rock type analog	Cohesion τ_0 (MPa)	Angle of internal friction (°)	Limiting§ stress state (MPa) $\bar{\sigma}_V$	$\bar{\sigma}_{NS}$	$\bar{\sigma}_{EW}$	Limiting‖ elastic strain ε_{xx} (%)
Bear River Formation (Lower Cretaceous) 6.9	1.9, 0.3, 8	Repetto siltstone	5	17	169	140	240	0.67
Gannett Formation (Jurassic–Cretaceous) 7.2	4.2, 0.2, 8	Repetto siltstone	5	17	176	130	230	0.30
Stump–Preuss (Jurassic) 7.4	5.7, 0.2, 10	Berea sandstone	20	29	102	140	320	0.32
Twin Creek Formation (Jurassic) 7.6	5.0, 0.3, 8	Solenhofen limestone	110	30–25	105	280	620	1.10
Nugget Formation (Triassic) 7.8	6.8, 0.2, 10	Tennessee sandstone	60	40–30	108	255	630	0.66
Ankareh Formation (Triassic) 8.0	6.8, 0.2, 8	Muddy shale	20	30–22	196	180	300	0.21
Thaynes Formation (Triassic) 8.3	5.1, 0.3, 8	Hasmark dolostone	32	43–25	115	260	525	0.94
Woodside–Dinwoody (Triassic) 8.7	6.8, 0.2, 8	Muddy shale	20	30–22	213	235	490	0.69
Phosphoria Formation (Permian) 8.8	7.6, 0.1, 8	Muddy shale	20	30–22	216	205	480	0.40
Weber Formation (Permo-Pennsylvanian) 8.9	7.6, 0.1, 10	Weber Sandstone	70	30	123	205	525	0.52
Morgan Formation (Pennsylvanian) 9.0	7.6, 0.1, 10	Muddy shale	20	30–22	221	205	440	0.34
Madison Formation (Mississippian) 9.3	7.4, 0.3, 8	Marianna limestone	20	30–20	129	170	350	0.13
Darby Formation (Devonian) 9.5	7.4, 0.3, 8	Hasmark dolostone	32	43–25	132	360	600	0.58
Bighorn Dolomite (Ordovician) 9.7	8.1, 0.3, 8	Blair dolostone	45	45	134	400	790	0.62
Gallatin Formation (Cambrian) 9.9	5.6, 0.3, 8	Solenhofen limestone	110	30–25	137	280	665	0.78
Gros Ventre Formation (Cambrian) 10.0	7.3, 0.1, 8	Muddy shale	20	30–25	245	180	380	0.52

* Depths of ramp footwall strata at time of ramp development based on data of Warner & Royse (1987).

† Young's modulus E and Poisson's ratio ν of non-carbonate rock types calculated with equations (31) and (32) from velocity data in Table 2. Young's modulus of carbonate rocks calculated from V_p data in Table 2, assuming that Poisson's ratio equals 0.3 in lieu of adequate V_s data. Values of the coefficient of thermal expansion α_T from Skinner (1966) are in units of $10^{-6}\,°C^{-1}$. Values of E are in units of 10^4 MPa.

‡ Strength data from Handin (1966), and from John Delphia and Jack Magourik of the Center for Tectonophysics, Texas A & M. Strengths of Twin Creek and Gallatin Formations, for example, are modeled with Solenhofen limestone because these formations contain fine crystalline or micritic limestones. Variations shown for the angle of internal friction are from low to high effective confining pressure.

§ Data of Handin (1966) indicate that strengths of sandstones, limestones and dolostones are reduced 10% or less for the temperature range under consideration, whereas strengths of Repetto siltstone and Muddy shale are reduced by 30% to 50% over this temperature range. An example is given in Fig. 9. Density for all units is assumed to be $\rho = 2500\ \text{kg m}^{-3}$.

‖ Figure 9 illustrates how limiting values are calculated with the fourth term of equation (33) for Nugget sandstone. For example, if Madison Formation had a strength equal to Hasmark dolostone instead of Marianna limestone, the strain value would have been closer to 0.46% instead of 0.13%.

Precise data for the elastic constants and strengths of footwall strata encompassed by the Hogsback ramp are not available yet. Estimates are based on other empirical data. For example, the elastic constants of the strata are estimated from equations (31) and (32) with velocity data from the Kemmerer region, using empirical relations between P-wave and S-wave velocities of specific rock types because only the P-wave velocities customarily are calculated during seismic profiling. However, modern computer programming capacities now enable both velocities to be determined on a routine basis (Thomsen 1986), and so more refined velocity data for thrust-belt analyses are to be expected in the not too distant future. In the meantime, the stratigraphic intervals in Table 1 are defined in terms of the velocity intervals currently available for the Kemmerer region in Table 2.

The potential failure states of stress, corresponding to a specific depth of each stratigraphic unit in the ramp footwall, are tabulated in Table 1. There, $\bar{\sigma}_{EW}$ is the subhorizontal effective principal stress in the easterly tectonic transport direction, with $\bar{\sigma}_{NS}$ as the effective principal stress in approximately the north–south direction and with $\bar{\sigma}_v$ as the effective overburden pressure. Each reference stress state is calculated from the first three terms of equation (33), assuming that $\delta = 0$ in lieu of adequate data. Each stress state for failure is estimated from Mohr envelope strength criteria of rock types similar to rock types in the ramp footwall. An example is given in Fig. 9. It shows the two contrasting stress states for the Nugget sandstone at a depth of 7.8 km. This value of depth y_0 in equation (33) is based on the analyses of Warner & Royse (1987) who show that erosion on the average had kept pace with thrusting of the Absaroka and Hogsback thrust sheets, with approximately 2.2 km of rock eroded since the emplacement of the Hogsback sheet.

The failure stresses in Table 1 enable limiting values of the elastic tectonic strain to be calculated for each stratigraphic unit in the manner illustrated in Fig. 9. This method is based on limit equilibrium mechanics, a standard procedure in soil mechanics and engineering rock mechanics to estimate upper limits of failure conditions when boundary-value problems cannot be formulated with precision (e.g. Lambe & Whitman 1979). From the standpoint of limit equilibrium mechanics, the strain values in Table 1 do not necessarily represent actual elastic tectonic strains required to induce shear failure in the ramp region. Instead, they indicate which stratigraphic units should be the first to undergo progressive failure.

Table 1 indicates that the massive dolomitic limestones of the Madison formation should be the first beds to undergo progressive failure, regardless of whether the tectonic elastic strain increases linearly with depth in the footwall strata or is constant with depth. However, if the Madison is more comparable in strength to the Hasmark dolostone than the Marianna limestone, then the critical relative value of the elastic tectonic strain of the Madison would be closer to 0.46% than to 0.13%. Shear failure development of the ramp accordingly would have been initiated nearly simultaneously in several incompetent units higher in the stratigraphic section of the predominantly competent sequence.

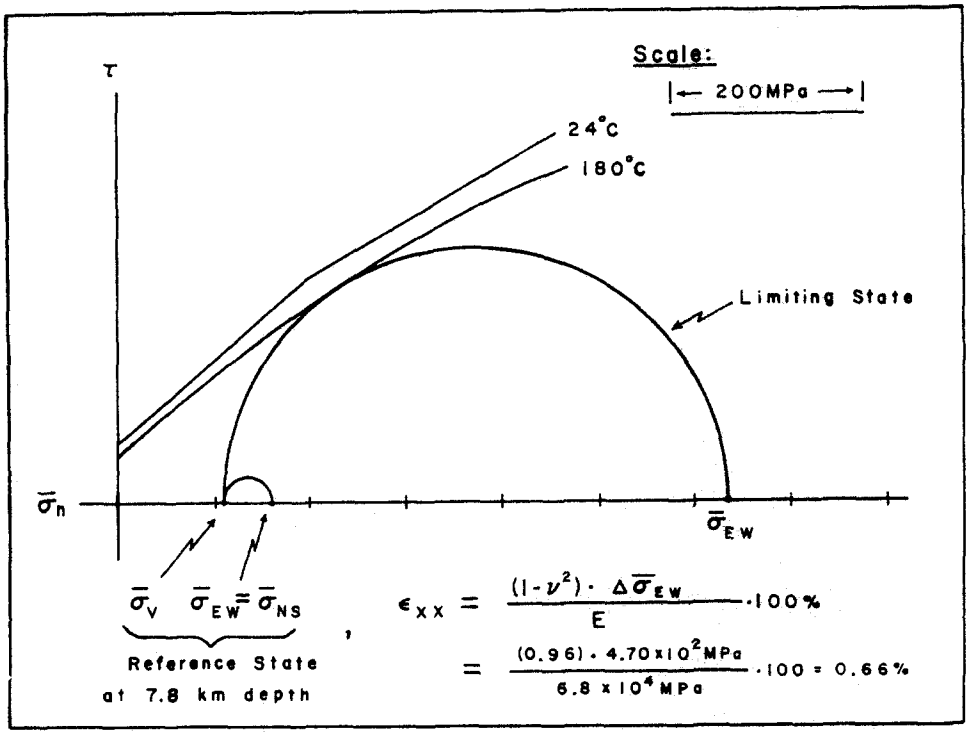

Fig. 9. Limit equilibrium anlaysis for shear fracture initiation of the Triassic Nugget sandstone at 7.8 km depth during development of Hogsback frontal ramp. A standard Hubbert–Rubey fluid pressure ratio of 0.435 and a geothermal gradient of 20°C km^{-1} are assumed. According to data of Handin (1966), the strength of competent sandstones is reduced 10% or less for the temperature range under consideration. The limiting value of 0.66% elastic tectonic strain at incipient failure is calculated from the fourth term of equation (33) and data in Table 1. See text.

Table 2. Stratigraphic and velocity data for calculation of elastic stiffnesses of strata along vertical sections h_2 and h_3 of Fig. 1, for the Kemmerer region of the Wyoming Salient

Stratigraphic interval	Section h_2 Thickness* (m)	V_p† (m sec^{-1})	V_s‡ (m sec^{-1})	Stiffness coefficient§ C (10^{13} N m^{-1})
Upper Cretaceous–early Tertiary	1300‖	3000	1400	2.0
Hilliard Formation (Upper Cretaceous)	2630¶	4000	2200	9.8
Frontier Formation (Upper Cretaceous)	850	3800	2100	2.6
Aspen Formation (Lower Cretaceous)	270	4500	2700	1.3
Bear River Formation (Lower Cretaceous)	240	3300	1700	0.5
Gannett Formation (Jurassic–Cretaceous)	300	4400	2600	1.3
Stump–Preuss (Jurassic)	180	5000	3100	1.1
Twin Creek Formation (Jurassic)	300	5200	2800**	1.7
Nugget–Dinwoody (Triassic)	890	5300	3400	6.1
Phosphoria (Permian) through Morgan (Pennsylvanian)	430	5600	3700	3.3
Madison Formation (Mississippian) through Darby (Devonian)	450	6300	3400**	3.6
Bighorn Dolomite (Ordovician)	150	6600	3500**	1.3
Gallatin–Gros Ventre (Cambrian)	370	5500	2900**	2.3
Sum of Coefficient‡‡ = 3.7×10^{14} N m^{-1}				

Stratigraphic interval	Section h_3 Thickness* (m)	Stiffness coefficient§ C (10^{13} N m^{-1})
Cretaceous–Tertiary	0	0
Hilliard Formation	610	2.3
Frontier Formation	850	2.6
Aspen Formation	240	1.1
Bear River	210	0.4
Gannett	270	1.2
Stump–Preuss	180	1.1
Twin Creek	300	1.7
Nugget–Dinwoody	910	6.2
Phosphoria through Morgan	400	3.1
Madison through Darby	430	3.5
Bighorn	150	1.3
Gallatin–Gros Ventre	370	2.3
— †† — — — — — — — — — — — — — — — — — —		
Gannett–Bear River	270	1.2
Stump–Preuss	150	0.9
Twin Creek	240	1.3
Nugget–Dinwoody	880	6.0
Phosphoria–Morgan	370	2.8
Madison–Darby	430	3.5
Bighorn	150	1.3
Gallatin–Gros Ventre	370	2.3
Sum of Coefficient‡‡ = 4.6×10^{14} N m^{-1}		

* Thicknesses determined from Plate 6 of Lamerson (1982) and from fig. 8D of Delphia & Bombolakis (1988) which shows a retrodeformed state that corresponds to the stage shown in Fig. 1. Densities are assumed to be 2500 kg m^{-3} for all strata in lieu of adequate data.

† Estimates of V_p obtained from several sources, courtesy of Champlin Petroleum Co. and Conoco Inc.

‡ Shear wave velocities calculated from empirical relations between V_p and V_s, given by Castagna *et al.* (1985). Exceptions in **.

§ In equation (34), $C = \dfrac{E_i}{1 - \nu_i^2} h_i$.

‖ Estimated from assumption that the ratio of total thickness along h_2 with respect to total thickness along h_3 remained approximately constant during Hogsback thrusting (cf. Warner & Royse 1987).

¶ The Hilliard clastics along section h_2 are overturned in the Lazeart syncline. Their vertical (apparent) thickness is estimated from the retrodeformed state in fig. 8D of Delphia & Bombolakis (1988), and from positions of unconformities in Plate 6 of Lamerson (1982).

** V_s for carbonate units calculated from V_p, with the assumption that Poisson's ratio = 0.30 in lieu of adequate data.

†† Dashed line demarcates the contact between hangingwall strata and footwall strata along section h_3.

‡‡ The summation is made with respect to equation (36), with the result that the ratio for h_3 with respect to h_2 is approximately 1.2.

Table 1 thus illustrates how the theory predicts which stratigraphic units undergo initial shear failure to develop a frontal ramp. The theory also predicts the amount of permanent strain induced within footwall strata along the ramp. Because the development of a frontal ramp by shear fracture should proceed in incremental stages during recurring slip of the geologic fault model, the total permanent strain within intact portions of ramp footwall rock should be in the range of 2–10% when pressure solution effects are not pervasive (see discussion of Bombolakis 1986, p. 286). This prediction is consistent with the twin lamellae measurements made thus far in ramp regions of foreland thrust plates. Spang *et al.* (1981), for example, calculate average strains of 5% from calcite and dolomite lamellae measurements in ramp regions of the McConnell thrust plate. The maximum principal strains were found to be subparallel to bedding, in the direction of tectonic transport.

It is still uncertain whether rupture length L of the fault model corresponds directly to the spacing between major frontal ramps. If a direct relation does exist, then equation (8) of Bombolakis (1986) predicts how several thrust-belt parameters affect the spacing. That analysis is necessarily oversimplified at this stage, and so further analyses of this important problem are required before various types of ramp spacing can be understood adequately. In the meantime, a problem that can be attacked more directly is the mechanical evolution of the imbricated ramp anticline in Fig. 8.

Delphia & Bombolakis (1988) demonstrate that most of the imbricates formed sequentially from east to west in the hinterland direction, thereby indicating that progressive locking of the upper plate developed in the ramp region. Since erosion on the average kept pace with thrusting of the Absoraka and Hogsback thrust sheets, the temperature and confining pressure gradients in Fig. 8 did not fluctuate in the manner usually hypothesized for rapid emplacement of thrust sheets (Warner & Royse 1987). Along each curved imbricate, there is a decrease of fault displacement upward, compensated by additional folding upward. Thus, if the imbrication were associated with seismic as well as aseismic modes of deformation, then the development of the imbricated ramp anticline would be consistent with the observation in continental seismic zones that aftershock and microseismic activity vary sporadically with depth, usually with pronounced decrease within a depth range of a few km of the topographic surface (Sibson 1983).

Therefore, we consider how laboratory studies and certain other field data indicate whether the imbrication of ramp anticlines involves seismic modes of deformation. A fundamental observation in laboratory studies of deformation is that contrasts in elastic stiffness between the loading system and the test specimen frequently determine whether failure proceeds in a quasi-stable or unstable manner (Cook 1981). If the stiffness of the loading system is appreciably greater than the stiffness of the specimen, then failure can proceed in a quasi-stable manner, regardless of whether the deformation is brittle or ductile. But if the stiffness of the loading system is approximately the same or less than the stiffness of the specimen, then failure can proceed in a more unstable manner with sudden stress drops. For this reason, a comparison of elastic stiffness is made with respect to the pattern of deformation in Fig. 8.

Suppose that Fig. 1 represents a precursory stage in the initial transformation of a simple ramp anticline into an imbricated ramp anticline (cf. fig. 5 of Boyer 1986). Each time recurring slip occurs along rupture length L, the thrust-belt segment stores an elastic strain in the stratigraphic sequence along h_2. The sequence along h_2 accordingly acts like a loading system that induces deformation in the ramp region over a time period that is large compared to the recurrence interval of seismic events along rupture length L. Thus, a comparison of the composite stiffness constants of the stratigraphic sequence along h_2 with respect to the duplicated sequence along h_3 should indicate whether seismic as well as aseismic modes of deformation would have occurred in the ramp region.

Strata data for these two sections with respect to the structure in Fig. 8 are tabulated for the Kemmerer region in Table 2. Using these data in equations (31), (32), (34) and (36), the ratio of the composite spring constants for h_3 with respect to h_2 is found to be in the range of 1.18–1.25. That is, the lithologic section along h_3 was approximately 1.2 times stiffer than the lithologic section along h_2. Since h_2 in Fig. 1 is analogous to a loading machine in the laboratory, h_3 is analogous to the middle section of a laboratory test specimen. During most laboratory experiments on brittle material, where the testing machine is not stiffer than the test specimen, the system comprising the machine and specimen becomes unstable at or near the peak of the stress–strain curve, resulting in violent failure due to rapid release of the relatively large amount of strain energy stored in the machine. As a rule of thumb, the ratio of the elastic energy in the machine to the strain energy in the specimen is more or less inversely proportional to the ratio of their spring constants (e.g. see equation 1 of Cook 1981). Therefore, since the ratio of the composite spring constants of h_3 with respect to h_2 was close to 1.2 in the Kemmerer region, seismic as well as aseismic modes of deformation probably did occur during imbrication of the ramp anticline in Fig. 8. The source of the elastic strain energy in front of h_2 in Fig. 1 therefore may have been recurring seismic and aseismic slip of the thrust-belt segment along rupture length L of the basal décollement.

Finally, despite the fact that the Lazeart syncline is adjacent to the Hogsback ramp, this fold actually is unrelated to the primary structure in the ramp region. Figure 10 shows the final stage of palinspastic restoration performed on fig. 8 of Delphia & Bombolakis (1988). Their analysis indicates that the Lazeart syncline had developed prior to the formation of the Hogsback frontal ramp. Apart from minor subsequent modifications, this major fold—more than 70 km in length—essentially had only gone along for the ride during Hogsback thrusting.

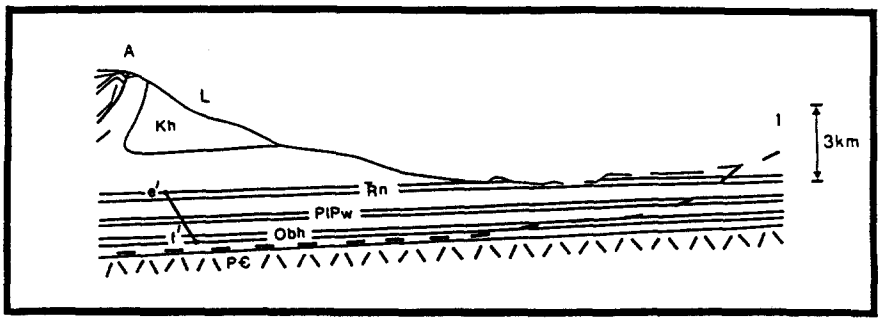

Fig. 10. Retrodeformed state of the structure in Fig. 8, prior to development of the Hogsback frontal ramp. Same notations as in Fig. 8. From Delphia & Bombolakis (1988).

CONCLUDING REMARKS

If recurring seismic slip occurs along a flat in a foreland belt, then transient elastic tectonic strains are imposed at the leading edge of the thrust-belt segment that has slipped. Their effects accordingly can be estimated with limit equilibrium mechanics. The appropriate choice of rheologic criteria depends on whether folding and flow are more prominent than brittle fracture and imbricate faulting. Regardless of the choice, there is no fundamental difference in the mode of analysis; only in the implementation, provided that recurring creep and seismic slip have occurred along a fault segment of the basal décollement.

Other parameters that need to be incorporated in subsequent analyses include the net slip variation along the strike of a thrust sheet, and the elastic shear stiffnesses of the strata, as well as the extensional and compressional elastic stiffnesses. They provide the data necessary to begin quantitative analyses of ramp development, imbrication and buckling. In each case, the elastic constants of differing strata within a sedimentary package are required. Because laboratory evaluation of the elastic constants is difficult and expensive, their evaluation from seismic velocity data is more suitable. The calculation of the elastic constants from seismic velocities, however, requires that appropriate values of the velocities be chosen. Seismic velocities tend to increase more or less with depth in a stratigraphic sequence. Thus, a given formation located at two different depths due to faulting or folding may exhibit two different sets of seismic velocities. The reason for this phenomenon appears to be selective closure of cracks, joints, and fractures as a function of effective confining pressure (O'Connell & Budiansky 1974). Consequently, a method needs to be developed in exploration geophysics whereby seismic velocity data are processed to take these factors into account. Then, some critical field data not previously utilized would be available for quantitative analyses of thrust-belt problems.

Acknowledgements—Helpful comments on a preliminary version of this paper were made by Stephen Bauer (Sandia National Laboratories), Peter D'Onfro, John Queen and Bill Rizer (Exploration Research & Development, Conoco Inc.), J. E. Ebel (Boston College), J. J. Gallagher (Arco Exploration & Technology Co.), R. J. Martin III (New England Res. Co. Inc), W. G. Pierce (U.S. Geological Survey), R. H. Riecker (White Rock, N. M.), Sandro Serra (Amoco Prod. Res.), Steven Wojtal (Oberlin College), Nick Woodward (University of Tennessee), and two anonymous reviewers. William Dupree and James Maloney of Boston College provided assistance with Tables 1 and 2. Cun-Hui Yang provided assistance with the derivation of the equations of the fault model. The efforts of Taffy Lynn Crider are much appreciated for the typing of a technically difficult manuscript, and in the arrangement of its format. Acknowledgement also is made to the donors of the Petroleum Research Fund, administrated by the American Chemical Society, for partial support of this research, and to NSF for support under Grant EAR-85 13029.

REFERENCES

Aki, K. 1983. Strong-motion seismology. In: *Earthquakes: Observation, Theory and Interpretation, Course LXXXV* (edited by Kanamori, H. & Boschi, E.). Proceedings of the International School of Physics "Enrico Fermi", Italian Physical Society. North-Holland, Amsterdam, 223–249.

Aki, K. 1984. Asperities, barriers, characteristic earthquakes, and strong motion prediction. *J. geophys. Res.* **89**, 5867–5872.

Allen, C. R. 1981. The modern San Andreas Fault. In: *The Geotectonic Development of California, Rubey Volume 1* (edited by Ernst, W. G.). Prentice-Hall, Englewood Cliffs, New Jersey, 512–534.

Armstrong, F. C. & Oriel, S. S. 1965. Tectonic development of Idaho–Wyoming–Utah thrust belt. *Bull. Am. Ass. Petrol. Geol.* **49**, 1847–1866.

Bauer, S. J., Holland, J. F. & Parrish, D. K. 1985. Implications about in situ stress at Yucca Mountain. In: *Proceedings of the 26th U.S. Symposium on Rock Mechanics* (edited by Ashworth, E.). A. A. Balkema Publishers, Cape Town, 1113–1120.

Berberian, M. 1982. Aftershock tectonics of the 1978 Tabas-e-Golshan (Iran) earthquake sequence: a documented active "thin-and-thick skinned tectonic" case. *Geophys. J. R. astr. Soc.* **68**, 499–530.

Bombolakis, E. G. 1981. Analysis of a horizontal catastrophic landslide. In: *Mechanical Behavior of Crustal Rocks. The Handin Volume* (edited by Carter, N. L., Friedman, M., Logan, J. M. & Stearns, D. W.). *Am. Geophys. Un. Geophys. Monogr.* **24**, 251–257.

Bombolakis, E. G. 1986. Thrust-fault mechanics and origin of a frontal ramp. *J. Struct. Geol.* **8**, 281–290.

Boyer, S. E. 1986. Styles of folding within thrust sheets: examples from the Appalachian and Rocky Mountains of the U.S.A. and Canada. *J. Struct. Geol.* **8**, 325–339.

Boyer, S. E. & Elliott, D. 1982. Thrust systems. *Bull. Am. Ass. Petrol. Geol.* **66**, 1196–1230.

Brune, J. N. 1968. Seismic moment, seismicity, and rate of slip along major fault zones. *J. geophys. Res.* **73**, 777–784.

Burchfiel, B. C., Wernicke, B., Willemin, J. H., Axen, G. J. & Cameron, C. S. 1982. A new type of décollement thrusting. *Nature* **300**, 513–595.

Castagna, J. P., Batzle, J. L. & Eastwood, R. L. 1985. Relationship between compressional-wave and shear-wave velocities in clastic silicate rocks. *Geophysics* **50**, 571–581.

Chapple, W. M. 1978. Mechanics of thin skinned fold-and-thrust belts. *Bull. geol. Soc. Am.* **89**, 1189–1198.

Chester, J. S. 1985. Deformation of layered rocks in the ramp regions of thrust faults: a study with rock models. Unpublished M.Sc. thesis, Texas A & M University.

Cook, N. G. W. 1981. Stiff testing machines, stick slip sliding, and the

stability of rock deformation. In: *Mechanical Behavior of Crustal Rocks, The Handin Volume* (edited by Carter, N. L., Friedman, M., Logan, J. M. & Stearns, D. W.). *Am. Geophys. Un. Geophys Monogr.* **24**, 93–102.

Dahlen, F. A., Suppe, J. & Davis, D. 1984. Mechanics of fold-and-thrust belts and accretionary wedges: cohesive Coulomb theory. *J. geophys. Res.* **89**, 10,087–10,101.

Dahlstrom, C. D. A. 1969. Balanced cross sections. *Can. J. Earth Sci.* **6**, 743–757.

Dahlstrom, C. D. A. 1970. Structural geology in the eastern margin of the Canadian Rocky Mountains. *Bull. Can. Petrol. Geol.* **18**, 332–406.

Davis, D., Suppe, J. & Dahlen, F. A. 1983. Mechanics of fold-and-thrust belts and accretionary wedges. *J. geophys. Res.* **88**, 1153–1172.

Delphia, J. & Bombolakis, E. G. 1988. Sequential development of a frontal ramp, imbricates, and a major fold in the Kemmerer region of the Wyoming thrust belt. In: *Geometries and Mechanisms of Thrusting, with special reference to the Appalachians* (edited by Mitra, G. & Wojtal, S.). *Spec. Pap. geol. Soc. Am.* **222**, 207–222.

Den Hartog, J. P. 1948. *Mechanics*. Dover, New York.

Den Hartog, J. P. 1956. *Mechanical Vibrations*. McGraw-Hill, New York.

Dixon, J. S. 1982. Regional structural synthesis, Wyoming salient of western overthrust belt. *Bull. Am. Ass. Petrol. Geol.* **66**, 1560–1580.

Eisenstadt, G. & De Paor, D. C. 1987. Alternative model of thrust-fault propagation. *Geology* **15**, 630–633.

Elliott, D. 1976a. The motion of thrust sheets. *J. geophys. Res.* **81**, 949–963.

Elliott, D. 1976b. The energy balance and deformation mechanisms of thrust sheets. *Phil. Trans. R. Soc. Lond.* **A282**, 289–312.

Elliott, D. 1980. Mechanics of thin-skinned fold-and-thrust belts: discussion. *Bull. geol. Soc. Am.* **91**, 185–187.

Frank, N. H. 1939. *Introduction to Mechanics and Heat* (2nd edn). McGraw-Hill, New York.

Gilotti, J. A. & Kumpulainen, R. 1986. Strain softening induced ductile flow in the Särv thrust sheet, Scandinavian Calendonides. *J. Struct. Geol.* **8**, 441–445.

Gretener, P. E. 1977. On the character of thrust faults with particular reference to the basal tongues. *Bull. Can. Petrol. Geol.* **25**, 110–122.

Haimson, B. C. 1977. Crustal stress in the continental United States as derived from hydrofracturing tests. In: *The Earth's Crust* (edited by Heacock, J. C.). *Am. Geophys. Un. Geophys. Monogr.* **20**, 576–592.

Handin, J. 1966. Strength and ductility. In: *Handbook of Physical Constants* (edited by Clark, S. P.). *Mem. geol. Soc. Am.* **97**, 223–289.

Hull, A. G. 1986. Late Pleistocene coseismic folding and associated faulting in coastal Hawke's bay, New Zealand. *Trans. Am. geophys. Un. (EOS)* **67**, 1224.

Jackson, J. A. 1983. The use of earthquake source studies in continental tectonic geology. In: *Earthquakes: Observation, Theory, and Interpretation, Course LXXXV* (edited by H. Kanamori & Boschi, E.). Proceedings of the International School of Physics "Enrico Fermi", Italian Physical Society. North-Holland, Amsterdam, 456–478.

Jaeger, J. C. & Cook, N. G. W. 1969. *Fundamentals of Rock Mechanics*. Methuen, London.

Kanamori, H. 1977. Quantification of earthquakes. *Nature* **271**, 411–414.

Kanamori, H. & Anderson, D. L. 1975. Theoretical basis of some empirical relations in seismology. *Bull. seis. Soc. Am.* **65**, 1073–1095.

King, G. C. P. & Vita-Finzi, C. 1981. Active folding in the Algerian earthquake of 10 October 1980. *Nature* **292**, 22–26.

Lambe, T. W. & Whitman, R. V. 1979. *Soil Mechanics. SI Version*. Wiley, New York.

Lamerson, P. R. 1982. The Fossil Basin and its relationship to the Absaroka thrust system, Wyoming and Utah. In: *Geologic Studies of the Cordilleran Thrust Belt, Volume I* (edited by Powers, R. B.). *Rocky Mountain Ass. of Geologists*, Denver, Colorado, 279–340.

Lamerson, P. R. 1985. Fossil Basin and its relationship to Absaroka thrust system, Wyoming and Utah. *Bull. Am. Ass. Petrol. Geol.* **69**, 853.

Logan, J. M. 1987. The brittle–ductile transition in experimental shear zones. *Trans. Am. geophys. Un. (EOS)* **68**, 1463.

McGarr, A. & Gay, N. C. 1978. State of stress in the earth's crust. *Annu. Rev. Earth & Planet. Sci.* **6**, 405–436.

Mitra, G. & Yonkee, W. A. 1985. Relationship of spaced cleavage to folds and thrusts in the Idaho–Wyoming–Utah thrust belt. *J. Struct. Geol.* **7**, 361–373.

Mitra, G. & Boyer, S. E. 1986. Energy balance and deformation mechanisms of duplexes. *J. Struct. Geol.* **8**, 291–304.

Mitra, S. 1986. Duplex structures and imbricate thrust systems: geometry, structural position, and hydrocarbon potential. *Bull. Am. Ass. Petrol. Geol.* **70**, 1087–1112.

Mogi, K. 1985. *Earthquake Prediction*. Academic Press, New York.

Murphy, G. M. 1960. *Ordinary Differential Equations and Their Solutions*. D. Van Nostrand Company, New York.

Namson, J. & Davis, T. 1988. Seismically active fold and thrust belt in the San Joaquin Valley, central California. *Bull. geol. Soc. Am.* **100**, 257–273.

Norton, M. A. 1983. Kemmerer area, Lincoln County, Wyoming. In: *Seismic Expression of Structural Styles, Volume 3*. Geology Series No. 15 (edited by Bally, A. W.), 3.4.1-45–3.4.1-47.

O'Connell, R. J. & Budiansky, B. 1974. Seismic velocities in dry and saturated cracked solids. *J. geophys. Res.* **79**, 5412–5426.

Pierce, W. G. 1987a. The case for tectonic denudation by the Heart Mountain fault—a response. *Bull. geol. Soc. Am.* **99**, 552–568.

Pierce, W. G. 1987b. Heart Mountain detachment fault and clastic dikes of fault breccia, and Heart Mountain break-away fault, Wyoming and Montana. *Geol. Soc. Am. Centennial Field Guide—Rocky Mountain Section*, 147–154.

Platt, J. P. & Leggett, J. K. 1986. Stratal extension in thrust footwalls, Makran accretionary prism: implications for thrust tectonics. *Bull. Am. Ass. Petrol. Geol.* **70**, 191–203.

Raleigh, B., Healy, J. H. & Bredehoeft, J. D. 1976. An experiment in earthquake control at Rangely, Colorado. *Science, Wash.* **191**, 1230–1237.

Ramsay, J. G. 1981. Tectonics of the Helvetic nappes. In: *Thrust and Nappe Tectonics* (edited by McClay, K. R. & Price, N. J.). *Spec. Publs. geol. Soc. Lond.* **9**, 293–309.

Roeder, D. H., Gilbert, O. E., Jr. & Witherspoon, W. D. 1978. Evolution and macroscopic structure of Valley and Ridge thrust belt, Tennessee and Virginia. *Studies in Geology* 2. Department of Geological Sciences, University of Tennessee.

Royse, F., Jr., Warner, M. A. & Reese, D. L. 1975. Thrust belt structural geometry and related problems, Wyoming–Idaho–northern Utah. In: *Symposium on Drilling Frontiers of the Central Rocky Mountains* (edited by Bolyard, D. W.). *Rocky Mountain Ass. of Geologists*, Denver, 41–54.

Rubey, W. W., Oriel, S. S., & Tracey, J. I., Jr. 1975. Geology of the Sage and Kemmerer 15-Minute Quadrangles, Lincoln County, Wyoming. *Prof. Pap. U.S. geol. Surv.* **855**, 1–18.

Savage, J. C. 1983. Strain accumulation in western United States. *Annu. Rev. Earth & Planet. Sci.* **11**, 11–43.

Schmid, S. M. 1975. The Glarus overthrust: field evidence and mechanical model. *Eclog. geol. Helv.* **68**, 247–280.

Schmid, S. M., Panozzo, R. & Bauer, S. 1987. Simple shear experiments on calcite rocks: rheology and microfabric. *J. Struct. Geol.* **9**, 747–778.

Schwartz, D. P. 1987. Earthquakes of the Holocene. *Am. geophys. Un. Rev. Geophys.* **25**, 1197–1202.

Schwartz, D. P. & Coppersmith, K. J. 1984. Fault behavior and characteristic earthquakes: examples from the Wasatch and San Andreas fault zones. *J. geophys. Res.* **89**, 5681–5698.

Schwartz, D. P. & Coppersmith, K. J. 1986. Seismic hazards: new trends in analysis using geologic data. In: *Active Tectonics*. National Academy Press, Washington, D.C., 215–230.

Serra, S. 1977. Styles of deformation in the ramp regions of overthrust faults. In: *Rocky Mountain Thrust Belt Geology and Resources* (edited by Heisey, E. L., Lawson, D. El, Norwood, E. R., Wach, P. H. & Hale, L. A.). *Joint Wyoming–Montana–Utah Geological Associatons Guidebook*, Wyoming Geological Association, 487–498.

Shimazaki, K. & Nakata, T. 1980. Time-predictable recurrence model for large earthquakes. *Geophys. Res. Lett.* **7**, 279–282.

Sibson, R. H. 1980. Power dissipation and stress levels on faults in the upper crust. *J. geophys. Res.* **85**, 6239–6247.

Sibson, R. H. 1983. Continental fault structure and the shallow earthquake source. *J. geol. Soc. Lond.* **140**, 741–767.

Sieh, K. E. 1981. A review of geologic evidence for recurrence times of large earthquakes. In: *Earthquake prediction, Maurice Ewing Series Volume 4* (edited by Simpson, D. W. & Richards, P. G.). *Am. geophys. Un. Geophys. Monogr.* 181–207.

Skinner, B. J. 1966. Thermal expansion. In: *Handbook of Physical Constants* (edited by Clark, S. P.) *Mem. geol. Soc. Am.* **97**, 75–96.

Spang, J. H., Wolcott, T. L. & Serra, S. 1981. Strain in ramp region of two minor thrusts, Southern California Rocky Mountains. In: *Mechanical Behavior of Crustal Rocks, The Handin Volume* (edited

by Carter, N. L., Friedman, M., Logan, J. M. & Stearns, D. W.). *Am. Geophys. Un. Geophys. Monogr.* **24**, 243–250.

Stein, R. S. 1986. Postseismic growth of the Coalinga fold. *Trans. Am. geophys. Un. (EOS)* **67**, 1223.

Stein, R. S. 1987. Contemporary plate motion and crustal deformation. *Am. geophys. Un. Rev. Geophysics* **25**, 855–863.

Stein, R. S. & King, G. C. P. 1984. Seismic potential revealed by surface folding: 1983 Coalinga, California, earthquake. *Science, Wash.* **224**, 869–872.

Stockmal, G. S. 1983. Modeling of large-scale accretionary wedge deformation. *J. geophys. Res.* **88**, 8271–8287.

Suppe, J. 1985. *Principles of Structural Geology*. Prentice-Hall, Englewood Cliffs, New Jersey.

Swan, F. H. 1987. Temporal clustering of paleoseismic events on the Oued Fodda fault, Algeria. In: *Directions in Paleoseismology* (edited by Crone, A. J. & Omdahl, E. M.). *U.S. Geological Survey Open File Report* **87–673**, 239–248.

Symon, K. R. 1971. *Mechanics* (3rd edn). Addison-Wesley, Reading, Massachusetts, U.S.A.

Thomsen, L. 1986. Weak elastic anisotropy. *Geophysics* **51**, 1954–1966.

Verrall, P., Dahlstrom, C. D. A. & Freund, H. 1981. *Structural Geology in the Canadian Overthrust Belt*. AAPG continuing education course. Am. Ass. Petrol. Geol., Tulsa, Oklahoma.

Warner, M. A. & Royse, F. 1987. Thrust faulting and hydrocarbon generation: discussion. *Bull. Am. Ass. Petrol. Geol.* **71**, 882–896.

Wentworth, C. M. & Zoback, M. D. 1986. An integrated model for the Coalinga earthquake: a guide to thrust deformation along the Coast Range–Great Valley boundary in Central California. *Trans. Am. geophys. Un. (EOS)* **67**, 1222.

Williams, W. D. & Dixon, J. S. 1985. Seismic interpretation of the Wyoming overthrust belt. In: *Seismic Explorations of the Rocky Mountain Region* (edited by Gries, R. R. & Dyer, R. C.). *Rocky Mountain Ass. of Geologists and Denver Geophysical Society*, 13–22.

Wiltschko, D. B. & Dorr, J. A., Jr. 1983. Timing of deformation in overthrust belt and foreland of Idaho, Wyoming and Utah. *Bull. Am. Ass. Petrol. Geol.* **67**, 1304–1322.

Wojtal, S. & Mitra, G. 1986. Strain hardening and strain softening in fault zones from foreland thrusts. *Bull. geol. Soc. Am.* **97**, 674–687.

Woodward, N. B. (Editor) 1985. *Valley and Ridge Thrust Belt: Balanced Structural Sections. Pennsylvania to Alabama. Appalachian Basin Industrial Associates*. Department of Geological Sciences Studies in Geology 12, University of Tennessee.

Woodward, N. B. 1987. Geological applicability of critical-wedge thrust-belt models. *Bull. geol. Soc. Am.* **99**, 827–832.

Woodward, N. B., Boyer, S. E. & Suppe, J. 1985. *An Outline of Balanced Cross-Sections* (2nd edn). Department of Geological Sciences Studies in Geology **11**, University of Tennessee.

Woodward, N. B., Wojtal, S., Paul, J. B. & Zadins, Z. Z. 1988. Partitioning of deformation within several external thrust zones of the Appalachian Orogen. *J. Geol.* **96**, 351–361.